3 Methods

3.1 Weather/Season scenario descriptions

For each farm scenario, we present results from six distinct 'seasonal patterns'. Two of these (September 1999 and March 2000) correspond to specific calendar periods – in the sense that the hydrodynamic model (which provides predictions of current speeds, water temperature etc. that are then used to drive the biological models) was driven using time series of winds and solar irradiance etc. for the indicated calendar periods. In the remaining four cases, the wind fields used to drive the hydrodynamic model are genuine time-series, but rather than applying them at the calendar times for which they were recorded, they have each been applied to both a spring- and a summer condition (in terms of irradiance and initial/boundary condition water temperatures etc.). The two wind-field time-series selected are considered to be representative of moderate-strong El Nino (prevailing winds from ENE; record corresponds to 21 February – 31 March 1962, measured at Mokohinau) or La Nina conditions (prevailing wind from WSW, record corresponds to 30 June to 30 July 1976, measured at Mokohinau) (Stephens, S.A. & Broekhuizen, N. 2003).

The spring and summer ENE (or WSW) hydrodynamic simulations were driven using the same wind-fields (though initial conditions, boundary conditions and solar irradiance differed). In the Snapper and logistic models, spring/summer differences in the results are due to seasonal changes in water-column stability (in the biophysical model, we also apply lower initial and boundary condition DIN concentrations in summer than in spring and appropriate diurnal irradiance patterns). Changes in water-column stability are driven by seasonal changes in the inputs of heat and fresh (riverine) water. In turn, this implies that the spring/summer ENE (or WSW) simulations provide an indication of how seasonal changes in water-column stability (rather than day-to-day weather changes) influence the dynamics of the planktonic ecosystem.

3.2 Farm Scenario Descriptions

We consider three distinct farm scenarios. The coordinates of the corners of the areas occupied by farms are listed in Table 1-Table 3. The co-ordinates were furnished by the Auckland Regional Council. Scenario NF is a baseline scenario in which no farms are present within the model's domain. Scenario 0 includes the existing farm at Waimangu Point and the two Wilson Bay developments. The many smaller mussel farms around the Coromandel Peninsula and in the Tamaki Strait are not represented. Scenario 1 is designed to examine the influence of an AMA operating at the 'maximum' extent that might be contemplated. In addition to the farms of Scenario 0,

an additional large block corresponding to the modelled AMA in the Western Firth is included.

Table 1:

NZ map grid coordinates of the corners of the two blocks (existing & approved) within the Wilson Bay development (coordinates provided by Auckland Regional Council).

Farm	Easting	Northing
Wilson Bay 1	2724703.000000	6475463.000000
Wilson Bay 1	2728084.000000	6470779.000000
Wilson Bay 1	2726594.611872	6469668.056505
Wilson Bay 1	2723196.261472	6474374.668749
Wilson Bay 2	2722381.715923	6473786.314924
Wilson Bay 2	2725789.355169	6469067.410723
Wilson Bay 2	2724298.000000	6467955.000000
Wilson Bay 2	2720875.000000	6472698.000000

Table 2:

NZ map grid coordinates of the corners of the nine existing blocks within the Waimangu Point development (coordinates provided by Auckland Regional Council).

Farm	Easting	Northing	Farm	Easting	Northing
Waimangu pt. 1	2714704.163357	6464623.553043	Waimangu pt. 5	2714988.227427	6465141.796762
Waimangu pt. 1	2714704.163357	6464410.158571	Waimangu pt. 6	2714989.613106	6464929.787968
Waimangu pt. 1	2714465.826673	6464408.772892	Waimangu pt. 6	2714748.505065	6464927.016611
Waimangu pt. 1	2714465.826673	6464620.781686	Waimangu pt. 6	2714745.733708	6465140.411084
Waimangu pt. 2	2714698.566969	6464878.094987	Waimangu pt. 6	2715261.439956	6464629.325229
Waimangu pt. 2	2714698.566969	6464677.068920	Waimangu pt. 7	2715258.927130	6464413.222207
Waimangu pt. 2	2714469.899818	6464674.556094	Waimangu pt. 7	2715038.111849	6464411.544249
Waimangu pt. 2	2714465.826673	6464875.746511	Waimangu pt. 7	2715038.111849	6464626.324400
Waimangu pt. 3	2714698.620643	6465139.025405	Waimangu pt. 7	2715266.748784	6464885.446259
Waimangu pt. 3	2714698.620643	6464925.630933	Waimangu pt. 8	2715266.465608	6464679.581746
Waimangu pt. 3	2714467.212352	6464924.245254	Waimangu pt. 8	2715038.111849	6464674.823144
Waimangu pt. 3	2714467.778678	6465137.546115	Waimangu pt. 8	2715035.340493	6464882.674903
Waimangu pt. 4	2714989.613106	6464626.324400	Waimangu pt. 9	2715268.134463	6465145.953797
Waimangu pt. 4	2714990.054766	6464413.222207	Waimangu pt. 9	2715268.978434	6464935.889981
Waimangu pt. 4	2714752.662100	6464411.544249	Waimangu pt. 9	2715035.340493	6464929.787968
Waimangu pt. 4	2714752.662100	6464624.938722	Waimangu pt. 9	2715035.340493	6465144.568119
Waimangu pt. 4	2714988.227427	6464881.289224			
Waimangu pt. 5	2714989.613106	6464677.594500			
Waimangu pt. 5	2714756.819136	6464676.208822			
Waimangu pt. 5	2714751.276422	6464878.517867			

Table 3:

NZ map grid coordinates of the corners defining the modelled maximal AMA in the western Firth of Thames (scenario 1) (coordinates provided by Auckland Regional Council).

Farm	Easting	Northing
Maximal WF AMA	2716619.225547	6466015.894963
Maximal WF AMA	2717473.826923	6465691.362795
Maximal WF AMA	2718512.329860	6464934.121070
Maximal WF AMA	2723088.233426	6461147.912446
Maximal WF AMA	2723465.272278	6456890.483937
Maximal WF AMA	2718199.855603	6457399.930948
Maximal WF AMA	2715504.998438	6465545.323320
Maximal WF AMA	2714401.589067	6465588.594275
Maximal WF AMA	2714423.224545	6466091.619135

3.3 Farm Details

3.3.1 Line Arrangements

The Wilson Bay AMA is divided into two sub-areas. Each is filled with numerous 2.75 ha "blocks". Each block is 250 m long and 110 m wide, and a "buffer" of 75 m separates neighbouring blocks. The blocks are stocked at a rate of two longlines per ha (equating to 5.5 longlines per block, or approximately 0.91 longlines ha^{-1} calculated over the area of the block and its associated buffer). Neighbouring longlines are separated by a gap of approximately 25 m.

The two sub-areas of development within the Wilson Bay AMA do not occupy the entire area of the AMA. When calculated over the entire area of the AMA, the effective line density is approximately 0.79 lines ha^{-1}.

In the absence of specific information, it was agreed to adopt the same configuration (0.91 lines ha^{-1}) within each of the nine existing farms at Waimangu Point.

For the modelled Western Firth AMA, it was agreed that no explicit provision be made for navigation passages etc. however implicit allowance is made for such structures by

setting the line-density to 0.79 lines ha^{-1} (equivalent to line density averaged over the entire Wilson Bay AMA).

An individual longline is assumed to have a length equalling that of the farm-block (250 m) less the projected horizontal length of the anchor cables at either end (a total decrement of six times the local water-depth). Each longline supports a double backbone and a total (summed over both backbones) of ~3000 m of dropper line per (2x) 130 m of backbone. It was agreed that we should assume that there would be no dropper lines where the water within the AMA is less than 10 m deep. Elsewhere, it was agreed, that for the purposes of modelling, it would be acceptable to assume that droppers extend to 8 m below the sea-surface.

The mussel population was assumed to be composed of five classes as outlined in **Table 4**. The line-density and mussel densities per line are such that, within the volume enclosed by the AMA (excluding water below the maximum dropper depth), there are approximately 4 mussels m^{-3}. Based upon measurements of size-dependent pumping rates, and the indicated population size structure, these four mussels could be expected to filter around 300 L of water a day. A naive interpretation of this clearance rate would imply that phytoplankton within the farm's boundaries suffer a mussel-induced mortality rate of ~30% d^{-1}. Note, however that this is an approximate upper bound on the incremental mortality. There are reasons to believe that, in reality it will be somewhat lower than this (see Discussion).

Table 4:

Details of the population size-structure and density within each farm. Note that approximately 10% of the total dropper line is assumed to be devoid of mussel.

Mussel Class	Shell-length (mm)	Mussels m^{-1} of dropper line	Proportion of dropper-lines
No mussels	-	-	0.1
'spat'	<35	170	0.2
'small juveniles'	35-60	150	0.23
'large juveniles'	60-85	130	0.23
'harvestable crop'	85-110	110	0.23

3.4 Model Domain

The horizontal domains of the three models extend from the southern tip of the Firth of Thames to just beyond the Tamaki Strait (**Figure 1**). The models explicitly represent the two Wilson Bay developments, the existing Waimangu point farms and modelled AMA. They do not represent the numerous smaller farms around the Coromandel Peninsula and Tamaki strait. In all our further illustrations, we restrict the plotted area

to a longitudinal band that encompasses the Firth of Thames; however, the models' domains extended as far as the western coastline of the Hauraki Gulf (i.e., they included the entire Tamaki Strait area and the Waitemata harbour area).

Figure 1:

Illustrations of the total horizontal extent of the domains used in (a) the snapper and logistic plankton models and (b) the biophysical model. The colour-coding is indicative of local water-depth.

a)

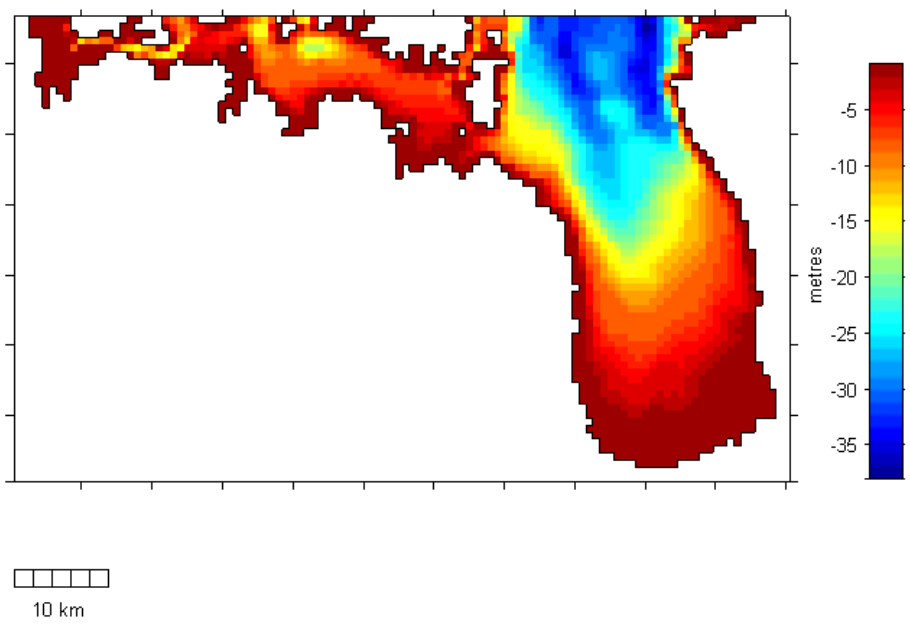

b)

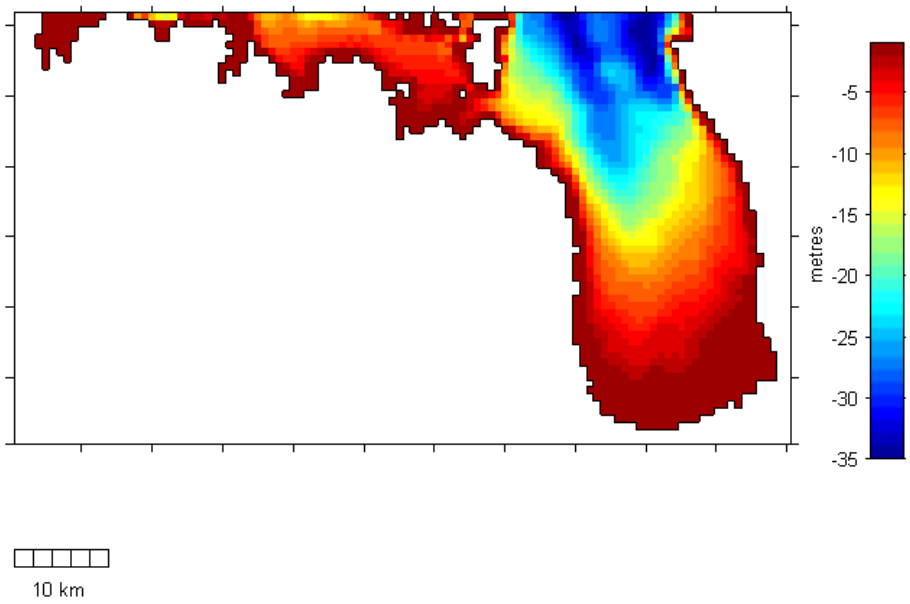

3.5 The Empirical Model

There is experimental evidence that the Greenshell mussel (*Perna canaliculus*) consumes not only phytoplankton, but also zooplankton up to at least the size (and mobility) of adult copepods (Zeldis, J. et al. in review). Adult copepods are of similar size to the eggs and young larvae of many fish (e.g., snapper eggs are 0.86-0.97 mm Robertson, D.A. 1975). They are also much more mobile than fish eggs. Thus, it is possible that *P. canaliculus* may consume the eggs and young larvae of fish – particularly given the experimental evidence that Blue mussel (*Mytilus edulis*) do so (Davenport, J. et al. 2000, Lehane, C. & Davenport, J. 2002).

To make an assessment of the potential impacts of mussel feeding upon phytoplankton/zooplankton and fish eggs/larvae we developed a new, particle-tracking model. We will refer to this as the 'empirical model'. Whilst the empirical model describes the dynamics of both phytoplankton/zooplankton (based upon the logistic growth model) and fish eggs/larvae (parameterised as snapper), we will discuss the results for phytoplankton/zooplankton and for snapper separately in most cases. Where appropriate in this section, we will therefore refer to the empirical model as the 'logistic model', or the 'snapper model'. The logistic model is designed to capture the general demographic characteristics of a wide range of planktonic organisms – ranging from fast growing phytoplankton (period between cell-divisions ~1 day), through slow-growing phytoplankton and protozoans (period between cell divisions ~2 – 5 d) and up to fast and slow growing copepods (egg – adult period of 20 – 40 d).

In both the snapper and logistic plankton models, the populations (snapper or plankton) are partitioned across numerous individual particles. The movement of each particle is dictated by the instantaneous local currents (taken from the output of the hydrodynamic model (Stephens, S.A. & Broekhuizen, N. 2003)) and the intrinsic 'swimming behaviour' of the population in question (snapper are assumed to be weakly, positively buoyant). The plankton and snapper are treated as different types of particles. Each 'plankton particle' carries information regarding its current location and also the quantity (mass) of each of five plankton sub-classes that the particle 'contains'. Similarly, each snapper particle carries information regarding its location and the quantities (numbers of individuals) of five different snapper sub-classes that it is representative of. In addition, the 'age' of the snapper particle (time since the first egg entered the particle) is tracked. The natures of the five sub-classes of plankton associated with plankton and snapper particles differ, and are clarified below. Within any volume of water, the concentration of a particular plankton or snapper sub-class is derived by summing the appropriate sub-class quantity over all particles within the volume. Net population growth over a time-increment is calculated for each sub-class in turn on particle-by-particle basis and results in the particle being representative of a greater (or smaller) quantity of the sub-class. On occasions, particles may be split into two, or new particles formed. This is explained in greater detail below.

The demographic description underlying the dynamics of the phytoplankton/zooplankton population differs from that underlying the snapper population. The logistic plankton model is formulated in a manner similar to that described by Abraham (1998). Not only do we adopt his particle-tracking approach, but we also follow his lead by basing our description upon the well-known logistic equation. In the context of our particle-based model, this may be written:

$$\frac{dN}{dt} = rN\left(1 - \frac{\bar{N}}{k}\right) - fN \qquad \text{(Eq. 1)}$$

in which N (mass) is the sub-class-specific quantity of material associated with the particle and $\bar{N}$ is the local sub-class-specific population concentration (mass m^{-3}). The parameter r (d^{-1}) defines the maximum weight-specific growth rate of the organism and k (mass m^{-3}), defines the 'carrying capacity' of the environment. This is the local abundance to which the population would naturally grow in the absence of 'interventions' (in this model, current-driven transport & mussel farms). The 'parameter' f denotes the weight-specific mortality induced by the local mussel population. In the full model (*cf* Eq. 1) this rate is a complex function of temperature, particulate concentration, mussel size and local mussel abundance.

The realised weight-specific growth rate is a declining function of current local population abundance relative to the local carrying capacity. We have assumed that both r and k are time-invariant, but k is assumed to vary spatially according to a bivariate normal distribution. We adopted this assumption for two reasons. Firstly, it

represents a crude approximation to the field data (see Figures 13 and 16 of Broekhuizen et al. (2002)). Secondly, in the absence of farms, the deviations between the prescribed carrying capacity and the realised abundance provide an indication of how transport is influencing demographics – something which would not be apparent if a spatially invariant carrying capacity had been adopted.

The demographic description for snapper eggs/larvae is not based upon the logistic growth equation. Rather, we assumed that the rates of both recruitment (rate of production of new eggs) and 'background' (i.e., mussel independent) per-capita mortality are independent of the existing egg and larval densities. A track of each particle's 'age' (time since particle was formed) is kept. Newly spawned eggs pass into only those particles which are less than one day old (henceforth: "zero-age" particles); older particles gain no further recruits. Particles lose individual eggs/larvae as a result of: (a) a first order, age-dependent background mortality term, and (b) an additional loss due to grazing by mussels. This latter term is applied only to particles that are within a farm.

The instantaneous, local spawning rate is specified as an areal rate of egg-production (eggs m^{-2} d^{-1}). This is converted to a volumetric rate on the basis of the local water-depth and the appropriate quantity of eggs is added into each zero-age particle within the water-column in question. In order to make this addition, it is necessary to know the volume of water that is notionally associated with each zero-age particle. Furthermore, it is also necessary to ensure that the "total notional volume" associated with all of the zero-age particles within each control-volume equals this control-volume. This is checked between each time-step, and, if necessary additional particles are added (initially, these are devoid of eggs). If instead, the total notional-volume is too great, the volumes (but not population sizes) of each of the zero-age particles within the control-volume are rescaled. Finally, it is desirable that all the particles (of a given age-class) represent a similar number of eggs (Broekhuizen, N. et al. 2003). In order to promote this, particles are split into two equal halves (both egg-count and notional volume) whenever the population (of sub-class 2, see below) comes to exceed a prescribed maximum. Note, that since only particles of age less-than-one-day can "grow", it is only these particles that will ever be split. An analagous particle-splitting strategy is applied to a plankton-particle whenever the abundance of sub-class two of the particle exceeds a prescribed value.

We assumed that spawning takes place only in waters between 10 m and 30 m deep (Zeldis, J.R. & Francis, R.I.C.C. 1998), and only between 9 am and 3 pm. Over this interval the instantaneous rate of egg production is assumed to follow a sinusoidal pattern such that the depth integrated egg production rate amounts to 350 eggs m^{-2} d^{-1} (Zeldis, J.R. & Francis, R.I.C.C. 1998). The background mortality rate for eggs and larvae was set to 70% d^{-1} (Zeldis, J.R. & Francis, R.I.C.C. 1998).

Given the differing demographic descriptions, we maintain two separate populations of particles: one for phytoplankton/zooplankton and one for fish eggs/larvae. In both cases, there are 8 state variables associated with each particle. The first three are related to the particle's three spatial co-ordinates (distance (m) from the origin in the three orthogonal directions); however for greater numerical ease, we calculate 'cumulative location' (product of the number of individuals in the particle and the mean location of these eggs). The particle's location (mean location of the individuals) is a derived property. The latter five state variables correspond to population abundance (measured as mg C for phytoplankton/zooplankton and as individuals for fish eggs/larvae). For a phytoplankton/zooplankton particle, each of the latter five state variables corresponds to one of the nominal plankton types listed in Table 5. In contrast to the situation for phytoplankton/zooplankton, we have no experimental data with which to make an assessment of just how effectively mussels clear snapper eggs/larvae from the water-column. Thus, in the case of particles representing fish eggs/larvae the latter five state variables are representative of near-replicate fish populations. These replicate populations differ only in their susceptibility to being consumed by mussels. In ascending order of sub-class (descending order of vulnerability) these vulnerabilities are: 1.0, 0.5, 0.25, 0.13, 0.06 – i.e., they range from being as vulnerable to predation as are phytoplankton to being more resistant than adult copepods (Zeldis, J. et al. in review). We use the terms vulnerability and relative vulnerability synonymously to refer to the following ratio:

"Volume of water which a mussel must filter in order to consume 1 g of the prey-type in question, divided by the volume of water that it must filter in order to consume 1 g of phytoplankton, both types of prey being equally abundant (by mass) in the water".

The phytoplankton/zooplankton are assumed to be neutrally buoyant. In the default simulations, the snapper are assumed to be positively buoyant (rising at a speed of 1 m d^{-1}). We have no measurements of the rates at which eggs or larvae rise through the water-column, but Pankhurst et al. (1991) report that eggs and young (pre-motile) larvae accumulated near the surface of their incubation tanks.

We imposed a spatially varying, but temporally constant-concentration boundary condition along the 'northern' boundary of the domain; at the sea-floor and sea-surface we imposed a reflecting boundary condition for plankton and snapper. In the case of plankton, the oceanic boundary conditions were derived from the assumed bivariate normal carrying capacity. In the case of snapper, they were based upon the rules governing spawning, and subsequent background mortality, but ignored the dispersive effect of transport (i.e., there were no older snapper eggs/larvae in regions where the water was <10 m, or greater than 30 m deep, even though, in reality, transport may introduce larvae into such areas).

Table 5:

Characteristics of the five nominal phytoplankton/zooplankton types. The relative vulnerability figures are based upon Zeldis et al. (in review).

Nominal Plankton Type	Max. per-capita growth rate (d^{-1})	K_{max} (mg C m^{-3})	K_{min} (mg C m^{-3})	Rel. vulnerability to mussel filtering
Fast growing phytoplankton (nutrient & light saturated diatom)	2	100	20	1.0
Fast growing, relatively invulnerable protozoan	1	100	20	1.0
Moderately slow growing phytoplankton/protozoa	0.2	100	20	1.0
Fast-growing (small species) copepod under favourable growth conditions	0.05	50	10	0.3
Slow growing copepod (large species) under favourable growth conditions	0.025	50	10	0.2

It is worth noting that each of the five 'replicate' snapper sub-classes has a different vulnerability to mussel consumption. Consequently, the equations for the rates of change of location for zero-age (only) snapper-particles that are (or have been) within mussel farms are exact only for sub-class 3. This is because the rate of change of cumulative location is a function not only of the local particle position, but also of instantaneous number of eggs associated with the particle and the rate at which newly spawned eggs are introduced into the particle. For particles that are (or have been) within a farm, the five sub-classes will differ in size and the relative contribution of births and movement of already-existing-individuals to the resultant velocity of the 'average individual' will differ in each sub-class. Recall, however that we have chosen to place all five sub-populations on the same particle (thus forcing them to move in the same manner). We have chosen to frame the equations of state for location relative to the third sub-class because this class has an intermediate vulnerability to consumption by mussels. Given the purpose of this modelling exercise, and the relatively small amount of differential mortality which can accrue between the different sub-populations on a zero-age particle during the few hours over which spawning takes place, we regard this approximation as acceptable. The alternative would have been to simulate each sub-class on a different particle, with the accompanying increase in the number of equations to be solved (each particle would require differential equations for its x, y, and z-locations as well as one for its population size). Thus, in place of one particle carrying eight differential equations, one would require five particles, each carrying four differential equations.

3.6 The Biophysical Model

This model is described in detail elsewhere (Broekhuizen, N. 1999, Broekhuizen, N. et al. 2003). Here, we present only a brief description and concentrate upon those parts of the model which have been modified since the model was described in the preceding publications. The principal modifications are:

- Addition of a third phytoplankton taxon (small phytoflagellates). These can represent more than 30% of the biomass at some times of the year (Chang, F.H. et al. in review). These are assumed to be neutrally buoyant and to require only nitrogen nutrient for growth (unlike diatoms, which also require silicon).
- Addition of an explicit pool of benthic organic detritus. Pelagic detritus now deposits onto the sea-floor and enters this benthic pool (rather than being reflected off the sea-floor as previously). Benthic detritus (like pelagic detritus) is assumed to decay into dissolved inorganic material at a rate of 5% per day, but 14% (Giles, H. 2001, Zeldis, J.R. & Smith, S.V. 1999) of the resultant DIN flux is assumed to be lost as N_2 (rather than recycled as NO_3 or NH_4^+).
- Addition of the mussel farms (see below).

Briefly, the model includes state variables for: local dissolved inorganic nitrogen (DIN), local dissolved reactive silicon (DRSi), local C, N and Si masses of organic detritus (POMC, POMN, POMSi), and for each of diatoms, phytoflagellates and dinoflagellates: numbers of cells, and C, N and Si biomass. Nutrients and organic detritus are simulated using the Eulerian approach, but we use the Lagrangian Ensemble method (Woods, J.D. & Onken, R. 1982) to describe the phytoplankton populations.

Cell division is assumed to take place when the cell surpasses a prescribed carbon mass ($W_{fission}$, mg C cell^{-1}). Each daughter cell is assumed to inherit half the mass of the parent. Starvation-death occurs should the cell's carbon mass fall below a prescribed minimum ($W_{starve} < 0.5\ W_{fission}$). In addition to discrete birth and death events related to a cell's physiological state, the phytoplankton populations are also assumed to suffer 'background' mortality (grazing and bacterial/viral lysis). This is implemented as a first order loss (note, this is a continuous loss, *c.f.* changes due to birth and starvation). The model of cellular growth incorporates terms reflecting quota-dependent regulation of the rates of excretion, photosynthesis and nutrient uptake, but lacks any photo-inhibition terms.

Ensemble-specific rates of photosynthesis and nutrient uptake etc. are calculated from the product of ensemble-carbon-biomass and the cell's mass-specific photosynthetic and nutrient-specific uptake rates etc. Local (to the particle ensemble) environmental conditions (orthogonal currents, temperature, light, nutrient concentrations etc.) are interpolated from the corresponding Eulerian field (in the vertical dimension only, except for orthogonal current vectors, which are interpolated in the x-, y-, or z-

directions as appropriate). Within each control-volume, we assume that the 'red' and 'green' light fractions decay exponentially (Taylor, A.H. et al. 1991 – the colour-specific attenuation coefficients are calculated as the sums of background- and phytoplankton-carbon terms). For all other characteristics, we use linear interpolation.

The light-dependence of photosynthesis is described using the Smith-formulation (Smith, E.L. 1936), however the realised photosynthetic rate becomes suppressed below the light-dependent rate as the nutrient quota (dinoflagellates and phytoflagellates N:C; diatoms N:C or Si:C) ratio approaches prescribed minima. Similarly, the nutrient uptake rate is dependent upon both the external nutrient concentration (Michaelis-Menten function) and the internal N:C (Si:C) ratio of the cell.

Dinoflagellates are assumed to swim upward (15 m d^{-1}) unless their N:C quota becomes sufficiently depleted. When this occurs, they switch to swimming downwards. They continue swimming downwards until: (a) their stores are sufficiently replenished (a second, higher N:C threshold), (b) the (external) nutrient-concentration dependent nutrient-uptake rate exceeds 90% of the maximum nutrient uptake rate, or (c), the cell comes within one meter of the sea-floor. Under condition (a), the cells will once again begin to swim upwards, under conditions (b) and (c), they will endeavour to remain (vertically) stationary. Diatoms cannot swim, but they are able to regulate their buoyancy (Smayda, T.J. 1970, Villareal, T.A. 1992). We assume that their buoyancy behaviour is analogous to the swimming behaviour of the dinoflagellates: As with the dinoflagellates, we assume that they endeavour to ascend (i.e., are neutrally buoyant) when nutrient replete (N and Si), but sink (5 m d^{-1}) when they are N- or Si- stressed. Phytoflagellates are assumed to be neutrally buoyant at all times.

The carbon and nitrogen fractions of organic detritus are assumed to decay into inorganic forms at rates of 5% d^{-1} (Enríquez, S. et al. 1993, Verity, P.G. et al. 2000). Detrital Si is assumed to decay at a much lower, temperature-dependent rate (~0.0006 d-1 at 20 C Kamatani, A. 1982, Tréguer, P. et al. 1989). As noted previously, 14% of the DIN remineralising from benthic detritus is assumed to be lost from the system as N_2.

We held the concentrations of nutrients, detritus and each of the three phytoplankton groups constant at the model's 'northern' boundary and imposed a reflecting boundary condition for phytoplankton at the sea-floor. In contrast, we adopted a 'sticky' sea-floor boundary condition for detrital material (material which comes sufficiently close to the sea-floor becomes immobilised on the sea-floor but remains biologically active).

3.7 Mussel Feeding sub-model

The rate at which a mussel removes particulates from the water-column is governed by the mussel's clearance rate (rate at which water is cleared of particles). Experimental data indicate that the clearance rate is determined by four factors: body size, total particulate concentration (incl. sediment), concentration of organic particulates and temperature (Hawkins, A.J.S. et al. 1999, James, M.R. et al. 2001 Unpublished NIWA data). Qualitatively: clearance is maximal at intermediate temperatures, increases quadratically with mussel length and is maximal at intermediate particle concentrations. Not all of the material which is initially removed from the water-column is subsequently ingested – some is rejected as pseudofaeces. The ingestion rate of food was modelled as a function of clearance rate, total particulate concentration, concentration of organic particulates and selective ingestion of food particles. In the empirical model, the concentration of food particles (as dry weight) was calculated as the sum of the concentrations of the five plankton sub-classes and the biomass of all age-classes of the snapper (weight-age relationship from Fielder, D.S. et al. in review and unpublished data from D.S. Fielder). In the biophysical model, the concentration of food particles was calculated as the sum of the three phytoplankton concentrations and the detrital concentration.

In the case of the Biophysical Model, it is also necessary to take proper account of the influence which mussels have upon the abundance of inorganic nutrients and detritus. Detrital consumption is calculated in the same manner as phytoplankton consumption. Detrital production is the sum of the production rates for pseudofaeces and faeces.

In the model, mussels are assumed to excrete dissolved inorganic nitrogen (as NH_4^+) as a consequence of two distinct processes. Firstly, there is a 'background', or 'basal' excretion rate. *In-situ* respiration and basal excretion rates (respectively mmol O_2 individual h^{-1}, and mg NH_4 individual^{-1} h^{-1}) have been measured for a range of mussel body sizes under normal feeding conditions and we adopt the size and temperature dependent rates derived from these data (Hawkins, A.J.S. et al. 1999, James, M.R. et al. 2001, NIWA unpublished data). Secondly, we assume that mussels maintain a fixed bodily N:C ratio. When the N:C ratio of their net assimilate (less excretion as calculated above) exceeds that of the body, the excess N must be excreted (as NH_4^+; conversely, if the N:C ratio of the net assimilate is less than that of the body, the excess carbon must be excreted – we assume this is excreted as dissolved inorganic carbon). In practise, this regulatory excretion is negligible in comparison with the basal term.

The basal term is based upon the experimentally derived rates, but we emphasize that, in the model, it is implemented in a non-conservative manner: the mussels excrete DIN at experimentally observed rates indefinitely and regardless of the quantity of nitrogen they are consuming. In reality, the rate of nitrogen excretion cannot exceed the rate of nitrogen consumption indefinitely. Conversely, if a factor other than

nitrogen limits mussel growth, the nitrogen excretion rate (or assimilation rate) must eventually rise in order that the mussel does not become impossibly nitrogen rich. In order to examine the model's sensitivity to the rate of mussel nitrogen excretion, we made some simulations in which the mussels were assumed to excrete only as much nitrogen (or carbon) as was required in order that they maintain a fixed internal N:C ratio (*ie* we retained the second, homeostatic excretion term, but turned off the first, so-called basal term). Nitrogen is conserved in this variant of the model.

3.8 Implementing Farms within the simulation models

The model has a horizontal grid-resolution of 750 m (56.25 ha). In the vertical, layers are of differing thickness (from the surface downwards: 3 m, 3 x 2m, 4 x 4 m, 2 x 8 m, 16 m). Henceforth, we will use the term 'grid-cell' or 'water-column' to refer to any such 750 m x 750 m column of water. We will use the term 'control-volume' to refer to a 750 x 750 x layer-depth cell. Clearly, the model does not represent scales as fine as one farm block (2.75 ha). Instead, we will consider any mussels to be dispersed evenly (between the sea-surface and maximal dropper depth) throughout the 56.25 ha.

We assumed all backbones support 3000 m of dropper line (this amounts to assuming that the water-depth is 20 m, so that within a 250 m long block, there a backbone 130 m long (250-6*20)). We assumed that the droppers extend to a depth of 8 m.

At the outset of each simulation, the fraction of each grid-cell which contains a farm is calculated as follows:

- we determined which grid-cells are entirely enclosed within a farm and assign these a fractional occupancy of 1 (less any fraction of the grid-cell which extends below the dropper-line depth);
- for those grid-cells which are not fully contained within a farm, we counted the number of grid-cell corners which are within a farm and assign the fractional occupancy as 0, 0.25, 0.5 or 0.75 as appropriate (less any fraction of the grid-cell which extends below the dropper-line depth);
- finally, we determined whether there were any farms which do not contain any grid-cell corners (because the farms are too small to span an entire grid-cell, or because the farm is aligned with the grid, and too narrow to span more than one grid-cell, so that even though it is longer than any one cell, the farm contains no grid-cell corners). We make this test by counting the number of farm corners within each of the as-yet-seemingly-unoccupied grid-cells. Cells containing one or more corners are (arbitrarily) assumed to be 10% occupied.

3.9 Numerical Solution

The system of differential equations was solved using a second order, adaptive time-step, Runge-Kutta integration algorithm with a maximum time-step of 30 minutes. After each time-step a check was made for the occurrence of any discrete events (e.g., passage of a particle from one water-column into a neighbouring one, and cell fission). Such events were arranged in estimated chronological order and processed appropriately. In addition, particles which had become 'too large' (see preceding section) were split. Finally, before beginning the next time-step, each particle was visited and a determination made of whether or not it was inside the boundaries of any of the farms. When within a farm, the particle's population suffered the appropriate additional mortality loss due to mussel feeding.

3.10 Simulations undertaken

For each of the three models we made a total of 18 (6 season/wind combinations x 3 farm scenarios) 'baseline' simulations. In addition, we made several additional simulations. These represent a very limited parameter sensitivity analysis. In the case of the snapper and logistic plankton models, these additional simulations were made only for the spring and summer ENE wind conditions. These are the conditions which promote the greatest retention of plankton within the firth, so making impacts most likely. Specifically, the additional simulations were:

- snapper assumed to rise at 5 m d^{-1} rather than rising at 1 m d^{-1}; relative vulnerability of plankton sub-classes 4 and 5 increased from 0.3, 0.2 to 0.5,0.3 respectively;
- snapper assumed to be neutrally buoyant rather than rising at 5 m d^{-1}; relative vulnerability of plankton sub-classes 4 and 5 increased from 0.3, 0.2 to 0.5,0.3 respectively.

In the case of the biophysical model, our alternative simulations concentrated upon the summertime period (when DIN limits phytoplankton growth). Specifically, we made simulations in which mussel N-excretion was reduced (such that excretion occurs only when absolutely required to maintain the N:C ratio) or eliminated entirely. These trials were made because the summertime phytoplankton enhancement predicted in the default simulations is dependent upon mussel-derived DIN, yet it is possible that the manipulations required to measure the mussel excretion rates that form the basis of DIN-excretion in the default simulations may have stressed the mussels causing them to excrete more N than usual (A.H. Ross, NIWA, *pers. comm.*). Thus, it was felt appropriate to determine what would happen if lower excretion rates are the norm.

In addition to the simulations examining the influence of changing DIN excretion, we have repeated the default-parameterisation summertime simulations, but using higher initial- and boundary condition DIN concentration. Our default value was 1 mg N m^{-3}

but we also present a summary of summertime results based upon simulations using initial and boundary conditions of 10 mg N m^{-3} (as used for the spring simulations).

Each simulation spanned a period between 19 and 25 d (see x-axis, Figure 12). Where the simulations were less than 25 d long, this was because the hydrodynamic model failed prior to day 25.